



Contents lists available at ScienceDirect

Spectrochimica Acta Part A: Molecular and Biomolecular Spectroscopy

journal homepage: www.elsevier.com/locate/saa

Two-phase activated colorimetric and ratiometric fluorescent sensor for visual detection of phosgene via AIE coupled TICT processes

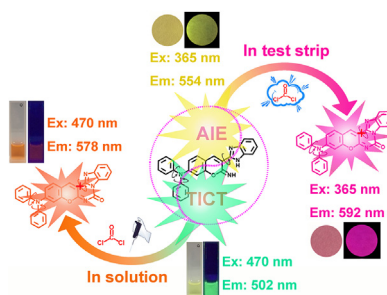
Qinghua Hu^{*,1}, Tao Gong¹, Yu Mao, Qiang Yin, Yuyuan Wang, Hongqing Wang^{*}

School of Chemistry and Chemical Engineering, Hunan Key Laboratory for the Design and Application of Actinide Complexes, University of South China, 28 Changsheng West Road, Hengyang, Hunan 421001, PR China

HIGHLIGHTS

- A colorimetric and ratiometric fluorescent sensor **DPA-CI** for phosgene sensing.
- **DPA-CI** can be activated in two-phase for visual detection of phosgene.
- **DPA-CI** showed excellent selectivity, rapid response, and fair sensitivity.
- **DPA-CI** loaded test strip for phosgene can be clearly observed by the naked eyes.

GRAPHICAL ABSTRACT



ARTICLE INFO

Article history:

Received 20 September 2020

Received in revised form 31 January 2021

Accepted 2 February 2021

Available online 16 February 2021

Keywords:

Fluorescent sensors

Phosgene

Ratiometric

AIE and TICT

Colorimetric

ABSTRACT

In this paper, we specifically designed and synthesized an excellent colorimetric and ratiometric fluorescent sensor **DPA-CI** for rapid and convenient detection of the highly toxic phosgene. **DPA-CI** was developed by incorporated a diphenylamine (DPA) and a 2-imine-3-benzo[d]imidazole as the enhanced push-pull electronic structure into the coumarin fluorophore matrix. The sensor **DPA-CI** towards phosgene sensing exhibited both visible colorimetric and ratiometric fluorescent color change in solution and in gaseous conditions with TICT and AIE mechanism respectively, which can be easily distinguished by using the naked eye. Also, the sensor **DPA-CI** showed splendid sensing performance such as excellent selectivity, rapid response (less than 8 s in THF and 2 min in gaseous condition), and fair sensitivity (limit of detection less than 0.11 ppm in gaseous condition and 0.27 μM in solution). The design strategy based on enhanced push-pull electronic structure with AIE and TICT properties will be helpful to construct a solid optical sensor with excellent potential application prospects for portable and visual sensing of gaseous phosgene through distinct color and ratiometric fluorescence change by the naked eyes.

© 2021 Elsevier B.V. All rights reserved.

1. Introduction

Phosgene, as a colorless, highly reactive poisonous gas, was the widespread use in the chemical industry, such as pharmaceuticals, synthetic polymers, chemical intermediates, pesticides, and dyes

synthesis [1–3]. As an insidious toxic gas, phosgene mainly damages the human respiratory system and has an incubation period of several hours before the toxic reaction occurs. Specifically, short-term exposure to more than 3 ppm of phosgene can irritate to the respiratory system, and exposure to 90 ppm for 0.5 h was fatal for humans [4–5]. Usually, the use of phosgene is tightly controlled. However, inadvertent leaks or intentional releases (such as biochemical weapons or terrorism) will seriously threaten the safety of human life [6–7]. Therefore, it's a pressing need to construct a fast, convenient, and sensitive monitoring method for

* Corresponding author.

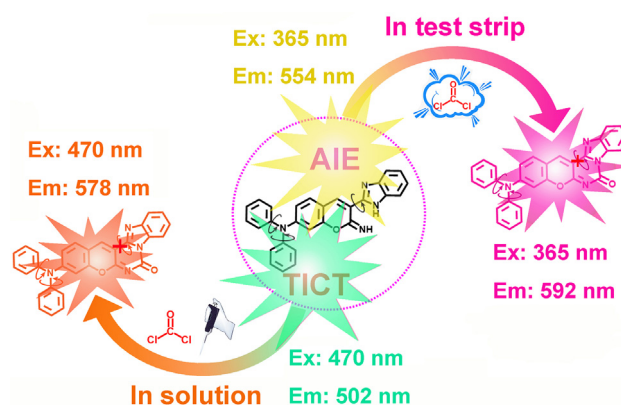
E-mail addresses: huqinghua2007@163.com (Q. Hu), hqwang2015@126.com (H. Wang).¹ These authors contributed equally to this work.

detecting small amounts of phosgene to stopping the damage in the early stages.

Compared to other large-scale instrument analysis methods for phosgene detection (such as GC, electrochemical analysis, and HPLC) [8–10], colorimetric and/or fluorescence sensors stand out with some unique advantages, for instance, simple implementation, low price, high sensitivity, and capable of on-site monitoring [11–29]. Up to now, reaction-based phosgene sensors are still the mainstream design idea, that the sensors reacted with phosgene can cause color and/or fluorescence change [30–55]. However, they mostly use the aggregation-caused quenching (ACQ) property dyes. Unfortunately, the ACQ dyes are not suitable for constructing solid-state sensors (test-strip or membrane sensors), their photoluminescence could be reduced in solid-state or their preparation was complicated, which will greatly affect the sensing performance.

On the contrary, in 2001, Tang and his coworkers discovered a new photoluminescence phenomenon was known as the aggregation-induced emission (AIE) [56]. AIE-based fluorophores showed very weak emission in diluted solutions but give off strong emission while forming aggregates or in solid-state conditions [57–68]. Therefore, AIE-based fluorophores could be more fit for the preparation of solid sensors, such as membrane sensors or test-strip. Nevertheless, AIE-based fluorophores with single-wavelength emitting can be affected by many factors, such as emitting light collection efficiency, exciting light intensity, and fluorescence probe concentration. Ratiometric fluorescent probe with dual-wavelength emission can effectively avoid these limitations, which provides built-in self-calibration for sensing process with higher sensitivity and accuracy [69–73]. Up to now, only two AIE-activated fluorescent solid sensors have been reported for phosgene sensing. In 2017, Wu's group reported the first AIE-activated test-strip sensing system for gaseous phosgene sensing [32]. Although the sensing system shows a ratiometric way, there are some obvious drawbacks, such as just a 21 nm wavelength shift after the reaction with phosgene, which will reduce the detection sensitivity caused by the spectral overlap. Meanwhile, almost no color change after the reaction was completed. Hence, colorimetric detection cannot be realized. Another AIE-based sensor for phosgene recognition is also not sensitive enough to satisfy the need for colorimetric detection due to the color just changes from creamy white to yellow [52]. As a result, it's of great significance and remains challenging to design AIE-based colorimetric and ratiometric fluorescent sensors with significant wavelength variations.

To improve the performance to satisfy the distinct color and ratio fluorescent sensing requirements for portable, sensitive, and visual sensing of phosgene. We herein designed a hopeful colorimetric and ratiometric fluorescent sensor (**DPA-CI**) for phosgene recognition by combined a strong electron-donor diphenylamine (DPA) and an electron acceptor (also used as the reactive group including two $-NH$ active site) 2-imine-3-benzo[d]imidazole, which incorporated the enhanced push-pull electronic structure into the coumarin fluorophore matrix. DPA moiety is considered as a strong electron-donor, which is beneficial to extend the π -conjugated system of the sensor molecule simultaneously to delocalize the electron distribution. Meanwhile, the conjugate of DPA moiety and the 3-benzo[d]imidazole group connected coumarin fluorophore matrix by the single bonds, both the DPA moiety and the 3-benzo[d]imidazole group have intramolecular rotation characteristics. Therefore, in our designed fluorescent sensor both AIE and TICT (twisted intramolecular charge transfer) effects could be observed. At the same time, the redshift of absorption and emission bands can be achieved by enhancing the push-pull electron effect. As illustrated in Scheme 1, the fluorescent sensor **DPA-CI** towards phosgene sensing can be realized in solution and solid-



Scheme 1. The proposed sensing mechanism of **DPA-CI** for phosgene in solution and in solid-state.

state with TICT and AIE mechanism respectively. Also, **DPA-CI** exhibits a fast response to phosgene (less than 8 s in THF and 2 min in a gaseous state), great selectivity and sensitivity (detection limit less than 0.11 ppm in gaseous condition and 0.027 μM in THF). The combined effect of AIE and TICT properties endows **DPA-CI** loaded test strip with excellent potential application prospects for on-site portable and visual phosgene sensing through distinct color and ratiometric fluorescence change in gaseous conditions.

2. Experimental sections

2.1. Material and general measurements

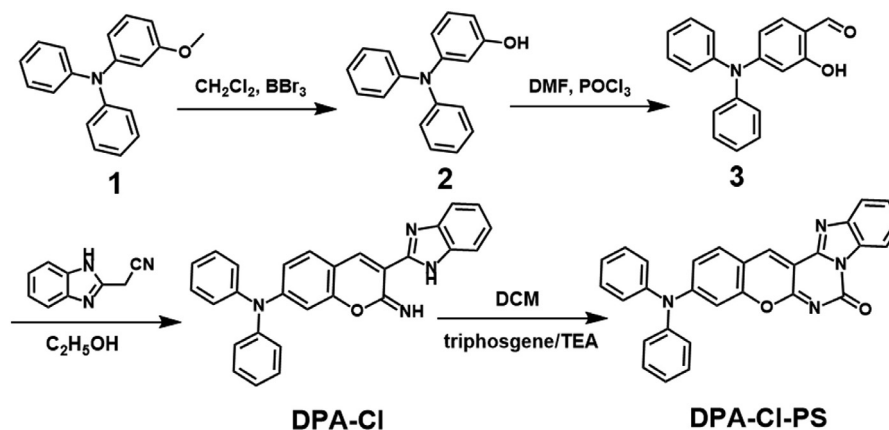
The reagents and solvents used in experiments were convenient to buy from some common commercial suppliers, such as Sigma-Aldrich, J&K Chemicals, Aladdin, or TCI, which were used directly does not require any further refinement. ^1H NMRs data were measured by using the Bruker 400 MHz and JEOL 400 MHz NMR Spectrometer by using CDCl_3 or $\text{DMSO}-d_6$ as the solvents. UV-Vis absorption spectra of the samples were tested on a U-3900 model (Hitachi) absorption spectrometer. Fluorescence spectra of the solutions and the test strips were tested on an F-7000 model (Hitachi) Fluorescence Spectrometer. ESI-HRMS data were collected through a Waters LCT Premier XE mass spectrometer. The fluorescence quantum yield and fluorescence lifetime data were recorded by using an Edinburgh FLS920 Full-featured fluorescence spectrometer. The size distribution was determined on a NanoBrook 90Plus Zeta analyzer at a fixed angle of 90° at 25°C . Transmission electronic microscopy (TEM) images of the sample were taken by a Hitachi HT7700 microscope.

2.2. Synthesis and characterization of the sensor

As described in Scheme 2, the probe **DPA-CI** can be easily synthesized in three steps.

2.2.1. Preparation and characterization of Compound 3

Compound 3 was prepared on the basis of previous report [74] in two steps as off-white solid with 64% yield. ^1H NMR (400 MHz, $\text{DMSO}-d_6$, Figure S1): δ 10.74 (s, 1H), 9.93 (s, 1H), 7.54–7.39 (m, 5H), 7.31–7.20 (m, 6H), 6.30 (dd, $J = 8.7, 2.2$ Hz, 1H), 6.20 (d, $J = 2.2$ Hz, 1H). HR-MS (ESI) $[M + H]^+$: $m/z = 290.1183$; Calculated: $\text{C}_{19}\text{H}_{15}\text{NO}_2 = 290.1136$.

Scheme 2. The synthetic procedure of **DPA-CI**.

2.2.2. Preparation of sensor **DPA-CI**

Compound 3 (0.4 mmol, 116 mg) and (2-benzimidazolyl) acetonitrile (0.4 mmol, 63 mg) was dissolved and transferred to a 50 mL pressure-resistant reaction tube with 15 mL ethanol, continue stirring for 30 min at room temperature, then 70 μ L piperidine was dropped in the reaction liquid. The mixture was allowed to heated and reflux for 2 h at 82 $^{\circ}$ C, a yellow product was precipitated out. After cooled, the sediment was filtered under reduced pressure and washed several times with absolute ethanol, a final light yellow solid power **DPA-CI** was obtained by drying under vacuum (154 mg, 90% yield). ^1H NMR (400 MHz, DMSO d_6 , Figure. S3): δ 12.94 (s, 1H), 10.49 (s, 1H), 8.46 (s, 1H), 8.11 (d, J = 8.9 Hz, 1H), 7.63 (d, J = 6.9 Hz, 1H), 7.45–7.41 (m, 5H), 7.24–7.20 (m, 7H), 6.68 (dd, J = 8.5, 2.2 Hz, 1H), 6.46 (d, J = 2.2 Hz, 1H), 6.41 (dd, J = 8.9, 2.3 Hz, 1H). ^{13}C NMR (400 MHz, CDCl_3 , Figure. S4): δ 157.90, 154.61, 151.64, 148.41, 146.18, 136.01, 129.84, 129.39, 126.28, 125.19, 122.71, 116.57, 112.81, 105.87. HR-MS (ESI) $[\text{M} + \text{H}]^+$: m/z = 397.1197; Calculated: $\text{C}_{28}\text{H}_{20}\text{N}_4\text{O}$ = 376.1463.

2.2.3. Preparation of **DPA-CI-PS**

The probe **DPA-CI** (0.3 mmol, 128 mg) and 606 mg Et_3N (6 mmol) was added into a 250 mL two-neck flask contained 100 mL dichloromethane, then the mixture was immersed into 0 $^{\circ}$ C ice bath. After stirred for 5 min under a N_2 atmosphere, then triphosgene (0.5 mmol, 149 mg) was completely dissolved in acetonitrile (15 mL) and slowly dripping into the reaction fluid with an injector. The reaction mixture was further stirred under room temperature over 10 h. Next, concentrated with reduced pressure distillation, the crude solid product was further purified by silica gel column using CH_2Cl_2 /methanol (v/v, 40/1) to yield a red powder **DPA-CI-PS** (125 mg, 92%). ^1H NMR (400 MHz, CDCl_3 , Figure. S6): δ 8.86 (s, 1H), 8.51 (dd, J = 6.4, 2.4 Hz, 1H), 7.83 (dd, J = 6.4, 2.2 Hz, 1H), 7.53 (d, J = 8.9 Hz, 1H), 7.43–7.48 (m, 5H), 7.34–7.26 (m, 7H), 7.02 (dd, J = 8.8, 2.2 Hz, 1H), 6.98 (d, J = 1.9 Hz, 1H). ^{13}C NMR (400 MHz, CDCl_3 , Figure. S7): δ 165.71.90, 155.63, 154.99, 152.02, 145.64, 144.56, 138.75, 130.70, 130.33, 127.08, 126.98, 125.55, 124.86, 119.26, 117.53, 115.79, 113.19, 106.03, 104.43, 100.00. HR-MS (ESI) $[\text{M} + \text{H}]^+$: m/z = 455.1505; Calculated: $\text{C}_{29}\text{H}_{18}\text{N}_4\text{O}_2$ = 454.1430.

2.3. Experimental Methods.

The stock solution (1×10^{-3} M) of **DPA-CI** and **DPA-CI-PS** were prepared by dissolving the solid in HPLC grade THF, while other analytes were dissolved in dichloromethane respectively. Optical studies (including UV-vis and fluorescent spectrum) were performed in HPLC grade THF, or the different proportions of water

and THF solutions at 25 $^{\circ}$ C, all the data were performed in standard fluorescent quartz cuvettes in size of 10.0 \times 10.0 mm. In our study, phosgene is produced by dropped a nonvolatile and less toxic triphosgene to the sensing system **DPA-CI** (10 μ M) in THF through the decomposition of triphosgene in the presence of 0.1% triethylamine (TEA).

2.4. Preparation of test strips with **DPA-CI**

The probe **DPA-CI** loaded test strips were prepared by immersing the filter papers (2 \times 5 cm) in the stock solution of **DPA-CI** (1×10^{-3} M) and taken out drying under air. The test strips can be stored in a dryer after preparation.

2.5. Detection of phosgene in solvents

In this part, triphosgene has been used as a precursor, which can be decomposed by trimethylamine(TEA) to generate phosgene in-situ. Spectrum response of phosgene in solution was conducted by adding different amounts of triphosgene stock solution into the THF sensor solution **DPA-CI** (10 μ M) containing 0.1% TEA at 25 $^{\circ}$ C. After a 1 min reaction, spectral changes in the emission spectra (λ_{ex} = 480 nm) and absorption (340 nm–580 nm) of the sensing system were then recorded in a fluorescence spectrophotometer and a UV-Vis spectrophotometer, respectively.

2.6. Phosgene sensing with test strips

Relative to other available materials, the commonly neutral filter paper is more suitable for preparing the sensing test strips. These paper strips were prepared by the method described previously and use directly. The different concentrations of gaseous phosgene were generated by mixing different amounts of triphosgene solutions in dichloromethane and 0.1% TEA in dichloromethane at the bottom of a sealed conical flask (200 mL). The test strips were hanged and exposed to these phosgene vapors and other analytes for 2 min. Then, taken out the test strip and recorded it on a fluorescence spectrophotometer (λ_{ex} = 365 nm). Meanwhile, a digital camera was used to collect the photos under visible light and a 365 nm hand-held lamp.

3. Results and discussion

3.1. Probe **DPA-CI** preparation and characterization

Compound 3 was obtained by using 3-Methoxytriphenylamine BBr_3 and POCl_3 as the reactant in two steps and finally produced an

off-white solid in 64% yield. For the synthesis of the probe **DPA-CI**, (2-benzimidazolyl)acetonitrile, and compound 3 were refluxed 1 h in ethanol with a catalytic amount of piperidine to obtain a yellow solid power with 90% yield. The probe **DPA-CI** can react efficiently with phosgene (generated by triphosgene with TEA) in DCM, giving an expected reference sensing product **DPA-CI-PS** in very good yield (92%). The structures of these three compounds were fully verified by ^1H NMR, ^{13}C NMR, and HR-MS(ESI) (as shown in Supplementary Data Figure S1-S8).

3.2. Optical properties measurement

In our design idea, we expect to obtain a sensor with AIE and TICT properties. To verify our thoughts, we tested the optical properties (including emission spectrum, fluorescence quantum yield, UV-vis absorption, and fluorescence lifetime) of the compounds **DPA-CI** and **DPA-CI-PS** in solution and solid condition. The sensor **DPA-CI** consists of a diphenylamine moiety which acts as a strong electron donor and 3-benzo[d]imidazole moiety is considered to be the electron-acceptor, which is connected by a rotatable single bond resulting in a twist propeller-like structure and incorporated the D- π -A push-pull electronic structure.

To confirm the TICT activity of the **DPA-CI**, the solvent polarity effect on the UV-vis absorption spectrum and fluorescence spectroscopy of **DPA-CI** was investigated. The good solubility of sensor **DPA-CI** in some familiar organic solvents such as EtOAc, chloroform, THF, DCM, DMF, DMSO, MeCN, and MeOH allows us to investigate the TICT activity in the solvents with different polarities, but it hardly soluble in water. The UV-Vis spectrum can be seen in Figure S9, the sensor **DPA-CI** has a peak at around 430 nm in THF, which changes little and exhibit quite a similar absorption peak in other polarity solvents. On the contrary, the fluorescent emission spectra of **DPA-CI** changed more obviously with the solvent polarity changed. As illustrated in Fig. 1A, the emission peaks varied gradually from 496 nm to 533 nm with the solvent polarity increased. Simultaneously, the emission intensity in chloroform and DCM were much higher than other solvents. These spectral data confirmed that the fluorescent properties of **DPA-CI** are significantly affected by the change of solvent polarity, which results from the TICT effect in the **DPA-CI** molecule with D- π -A structures. Moreover, a large Stokes shift over 100 nm was realized.

To further explored the impact of the polarity of the solvents on the photoluminescence spectra of **DPA-CI**, the emission maximum shift of **DPA-CI** in different solvents versus the $E_T(30)$ (solvent polarity empirical parameter) is plotted in Fig. 1B and the other related data were listed in Table S1. A linear relationship fitting was found with a good correlation coefficient ($R^2 = 0.986$) and a 3.72 slope was obtained between the emission maximum and $E_T(30)$, which showed a weak solvatochromism of **DPA-CI**. To further confirmed the TICT activity of the sensor **DPA-CI**. The solvatochromic properties of **DPA-CI** were further evaluated by the Lippert-Mataga equation of the $\Delta\nu$ (Stokes shift) versus Δf (solvent polarity parameter) for TICT molecules (Table S1 and Fig. S10). As shown in Fig. S10, the $\Delta\nu$ of each **DPA-CI** solvent increases with the increase of solvent polarity. A high slope of 8993.70 was obtained by the linear line, which shows the striking difference ($\Delta\mu$) between the μ_g (ground state dipole moment) and the μ_e (excited dipole moment). The results indicated that the charge separation exists in the **DPA-CI** structure and further confirmed the TICT assumption. Subsequently, the emission responding toward viscosity of **DPA-CI** in methanol and glycerol mixture was investigated. By adding the high viscosity glycerol into methanol solution, while the glycerol fraction (f_G) increase to 50%, the emission at 532 nm of **DPA-CI** was reduced gradually. In sharp contrast, as the f_G continues to rise to 100%, the emission of **DPA-CI** was enhanced (Figure S11 A and B). Meanwhile, the emission peak of **DPA-CI**

showed a red-shift from 532 nm to 558 nm, which could contribute to the TICT effect due to the suppressing rotation of diphenylamine moiety and 3-benzo[d]imidazole moiety in viscous media. Also, the TICT effect of **DPA-CI** can be explained in terms of DFT calculations under Gaussian 16 at the B3LYP/6-31G(d) basis set. As illustrated in Figure S12, the photoexcitation (electron clouds) from the HOMO to LUMO of **DPA-CI** involves an obvious ICT process from the diphenylamine unit to the 3-benzo[d]imidazole-chromen-2-imine unit. Since the phenylamine unit in the diphenylamine unit and the single bond between 3-benzimidazole and the chromen-2-imine unit are freely rotatable. So the previously mentioned ICT process is an actual TICT process formed by a significant molecular geometry change.

Besides the TICT activity, we also investigated the AIE behavior of **DPA-CI** and the sensing product **DPA-CI-PS**. The experiments were carried out by monitoring its emission spectra in mixture solvent systems (THF/water) with different fractions of water (f_w), which is a classic method applied to evaluate the AIE effect. As revealed in Fig. 2(A, C, E), **DPA-CI** shows an emission peak at 500 nm in THF with a quantum yield (Φ_f) of 24.4%. With the f_w increases from 0 to 99%, the peak intensity of **DPA-CI** decreased gradually, along with the maximum emission wavelength red-shift from 500 nm to 554 nm. This phenomenon could be caused by the TICT effect arising from the fraction of water increase. In comparison, **TPE-CI-PS** exhibits completely different photoluminescence properties. As shown in Fig. 2(B, D, F), **DPA-CI-PS** exhibit an orange light at around 570 nm in dilute THF solution with the Φ_f of 5.6%. However, when 10% of water added, the fluorescence intensity at 570 nm decreased dramatically. This fluorescence quenching effect could be explained as the TICT effect in the **DPA-CI-PS** solution due to the addition of water and increased solvent polarity. When the water fractions ranging from 10% to 70%, the fluorescence intensity of **DPA-CI-PS** continues to decrease slowly. Upon further increasing the f_w from 70% to 80%, a rapid enhance in the peak intensity at 592 nm together with a redshift in the peak emission wavelength from 570 nm to 592 nm was observed. Due to the poor solubility in the high water fractions THF solution, **DPA-CI-PS** will be aggregated and activates the AIE process. Surprisingly, when the f_w increased from 80% to 95%, the emission decreased rapidly. This phenomenon may be attributed to two possible factors [67]: (1) When the f_w above 80%, the excessive aggregation **DPA-CI-PS** molecules leads to the reduction of internal radiation, which results in a less emissive; (2) In a high f_w solution (above 80%) the sensor molecules may form more amorphous particles, which could decrease the emission intensity. To prove that assertion, the aggregation of 80% and 95% water fraction of **TP-CI-PS** was characterized by dynamic light scattering (DLS) and transmission electron microscopy (TEM). As shown in Figure S13A and S13B, the average hydrodynamic diameter is 112.56 ± 0.58 nm (f_w 80%) and 381.33 ± 0.78 nm (f_w 95%), respectively. The TEM images revealed good dispersion nanoparticles in the f_w of 80% (Figure S13C). While in the f_w of 95%, the dispersed nanoparticles produced significant aggregation (Figure S13D). Besides, we also measured and fitted the average fluorescence lifetimes (τ) of **DPA-CI** and **DPA-CI-PS** in THF, 80% f_w solution, and solid-state. As shown in Figure S14 and S15, the average fluorescence lifetimes of **DPA-CI** in THF, 80% f_w solution, and solid-state were fitted for 2.87 ns, 3.08 ns, and 1.79 ns at 554 nm, respectively. While the average fluorescence lifetimes of **DPA-CI-PS** in THF, 80% f_w solution, and solid-state at 592 nm were fitted as 7.19 ns, 9.03 ns, and 2.46 ns, respectively. The fluorescence quantum yields of **DPA-CI** and **DPA-CI-PS** in solid states were measured at 3.4% and 17.7% respectively, these results are consistent with the previous AIE behavior test results in THF/water mixture systems.

To have a better insight into the novel optical properties change of the sensing strategy, the trends in the frontier orbital distribu-

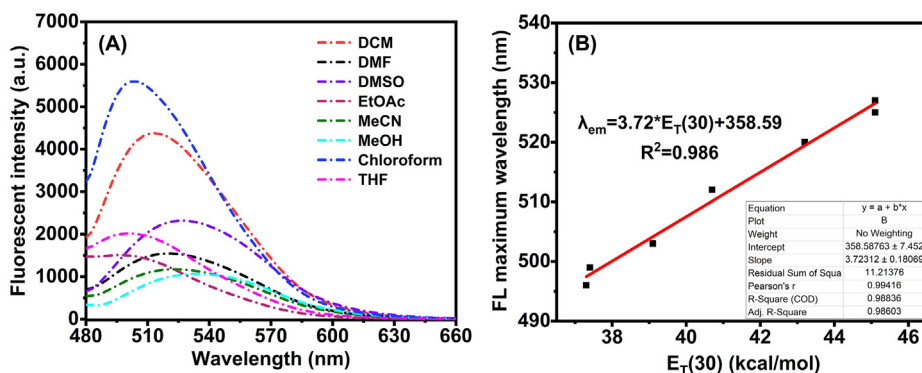


Fig. 1. (A) Fluorescent spectra of **DPA-CI** in different solvents. (B) The plot of the maximum emission peaks of **DPA-CI** in some common solvents versus each solvent polarity empirical parameter $E_T(30)$. Final concentration: 10 μ M; Excitation at 475 nm.

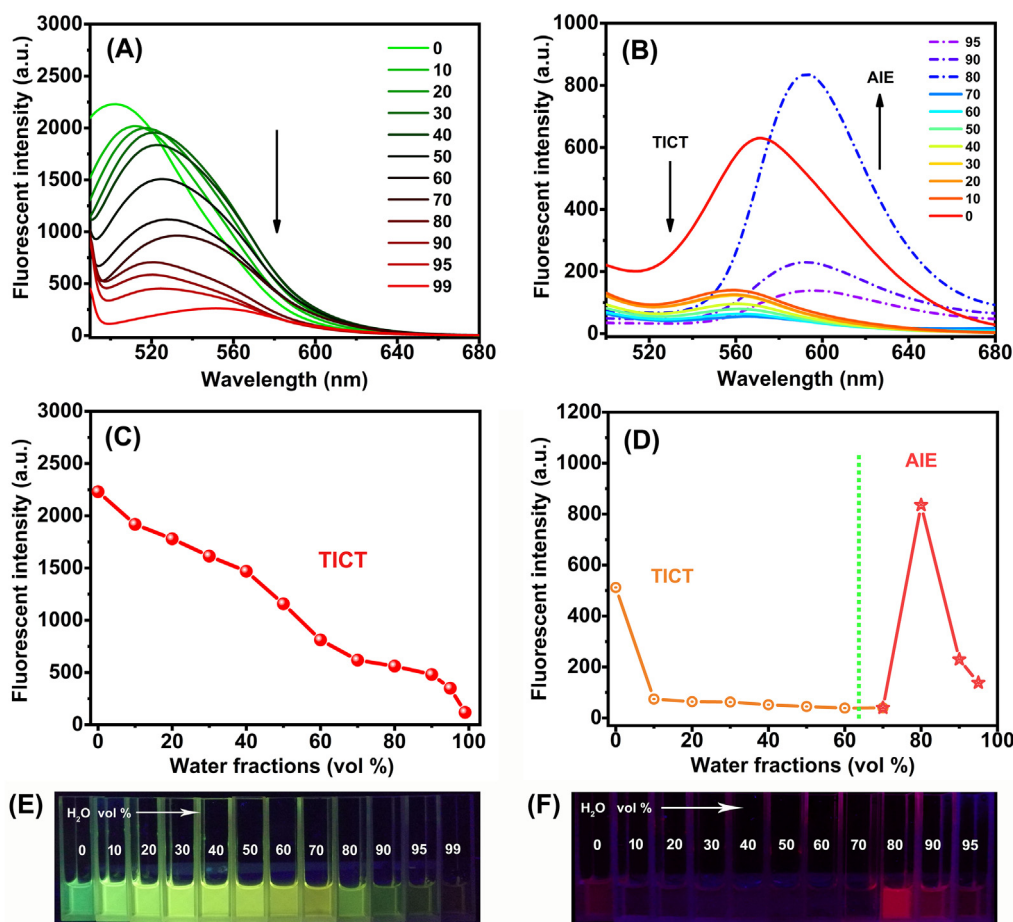


Fig. 2. Emission spectra of (A) **DPA-CI** and (B) **DPA-CI-PS** in THF/water mixture solvent systems with different fractions of water (f_w); The plot of maximum intensity versus different water fraction (f_w) of (C) **DPA-CI** (at 500 nm) and (D) **DPA-CI-PS** (at 592 nm); Fluorescent pictures of (E) **DPA-CI** and (F) **DPA-CI-PS** in THF/water mixture systems with the water fractions (f_w) increased. Final concentration: 10 μ M; excited at 475 nm.

tions and the electronic transition energies for **DPA-CI** and the expected sensing product **DPA-CI-PS** were optimized and calculated with the density functional theory (DFT) method. As illustrated in Fig. 3, the HOMO electron clouds of two optimized molecules were nearly uniformly distributed vertically over the π - π conjugation. While excited, on the LUMO of **DPA-CI**, just the electron clouds on the diphenylamine unit transferred to the iminocoumarin part, forming the TICT process. However, by comparison, we find that the TICT process on the LUMO of **DPA-CI-PS** was realized by transferring the most electron clouds from the

diphenylamine unit and 3-benzimidazole unit to the inocoumarin cyclic urea part. That because the inocoumarin cyclic urea structure in **DPA-CI-PS** was considered as a rigid planar, which inhibits single bond rotation between 3-benzimidazole and the iminocoumarin unit, and further enhanced the ICT effect and activate the AIE properties in **DPA-CI-PS**. In general, the enhanced ICT effect will cause a redshift in absorption wavelength and enhanced fluorescence-emission. Also, the supposed optical properties change was in qualitative support the HOMO-LUMO energy gap difference between **DPA-CI** (0.120 eV) and **DPA-CI-PS** (0.101 eV),

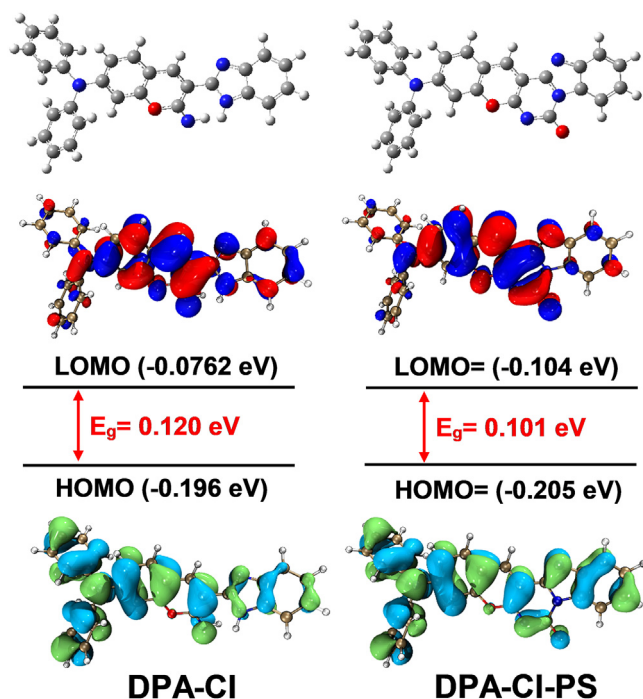


Fig. 3. Comparison of the frontier molecular orbitals of **DPA-CI** and **DPA-CI-PS** and the orbital energies.

which were following the red-shift of absorption peaks from 430 nm to 506 nm and the maximum emission peaks from 502 nm to 578 nm in solution.

3.3. Optical sensing experiments of **DPA-CI** in solution.

The optical sensing assays of **DPA-CI** were conducted by titrating various concentrations of triphosgene stock solution into the sensing solution of **DPA-CI** (10 μM) in THF at 25 $^{\circ}\text{C}$ containing 0.1% TEA. The changes in fluorescent emission ($\lambda_{\text{ex}} = 470 \text{ nm}$) and the absorption spectrum were monitored after the triphosgene was added for one minute. As shown in Fig. 4A, sensor **DPA-CI** in THF mainly showed a maximum absorption peak at 425 nm. With the triphosgene amount increasing, the absorption band at 425 nm gradually decreased, and a new absorption band at 506 nm gradually enhanced, which accompanied a noticeable color change from light yellow to orange (Fig. 4A, inset), showed a colorimetric sensing process. Then, we tested the fluorescence change of the sensor **DPA-CI** with phosgene. As expected, we can see in Fig. 4B, the sensor exhibited an excellent ratiometric fluorescence change to phosgene. With the phosgene concentrations increasing (0–200 μM), the maximum emission peak at 502 nm decreased dramatically along with a new emission band increased at 578 nm. A distinct fluorescence change from green to orange-red is easily identified under a 365 nm desk lamp (Fig. 4B, inset), indicating a ratiometric fluorescence detection process. These remarkable optical properties change could be ascribed to the phosgene induced cyclization reaction with the $-\text{NH}$ groups in 3-benzo[d]imidazole-chromen-2-imine unit to form hexatomic cyclic urea, which inhibited part of the TICT behavior and increasing the conjugate system. As illustrated in Fig. 4C, the ratio of the emission intensity at 578 and 502 nm (I_{578}/I_{502}) versus the increasing amount of phosgene from 0 to 90 μM showed an excellent linear relationship ($R^2 = 0.994$), and the LOD (limit of detection) was calculated as 0.27 μM (according to the formula $3\delta/k$). Meanwhile, the time-dependent studies showed that the peak intensity at 502 nm reaches a plateau within

8 s upon the triphosgene added (Fig. 4D). The above results showed that **DPA-CI** can be used as a colorimetric and ratiometric fluorescent sensor for phosgene sensing in THF solvent.

3.4. Sensing properties of **DPA-CI** in solid State.

Inspired by the promising optical properties in solution, since the phosgene is existing as a poisonous air pollutant, there is little point in identifying phosgene gas in solvents. So we need to established a method for the monitoring of gaseous phosgene. Compared with other types of solid-state based optical sensors, the paper-based test strip is simpler to prepare and convenient to use. Therefore, a new test strip was prepared by immersed a qualitative filter paper in the **DPA-CI** solution and take out to dry naturally. The gaseous phosgene was produced by mixing various concentrations of triphosgene and a proper amount of TEA in a cork-sealed conical flask. The test strips were suspended in the flask and exposed to phosgene vapors for 2 min, then recorded on a fluorimeter ($\lambda_{\text{ex}} = 365 \text{ nm}$). As shown in Fig. 5A, without the phosgene, the **DPA-CI** loaded test strip is initially emitted at around 554 nm. Upon exposure to phosgene, the peak intensity at 554 nm gradually dropped off, a new emission band at around 592 nm was generated and its intensity enhanced along with the phosgene concentration increasing. Therefore, the test strips in response to the gaseous phosgene also exhibited a ratiometric way. The redshift of the wavelength and the increasing emission intensity at 592 nm is due to the reaction between **DPA-CI** and phosgene. The formation of hexatomic cyclic urea inhibited the intramolecular rotation in the 3-benzimidazole part and further enhanced the AIE effect of the test strip. Moreover, as shown in Fig. 5B, in the range of 2–45 ppm, the ratio of $I_{592 \text{ nm}}/I_{554 \text{ nm}}$ versus the phosgene concentration existed good linearity ($R^2 = 0.996$). The limit of detection (LOD) of the test strip for gaseous phosgene sensing was calculated as low as 0.11 ppm according to the equation $3\sigma/k$, which was far below the critical concentration (20 ppm) that can result in immediate danger to human health [34]. To further demonstrate the promising application of **DPA-CI** for phosgene visual detection, the exposed test strips were photographed by a digital camera under a daylight lamp and a portable 365 nm lamp. As illustrated in Fig. 5C, with the phosgene level increasing, under a daylight lamp, the test strips color changed from yellow to peach, while under the 365 nm lamp, the emission color changed from light yellow to rose. The color change can be clearly distinguished by the naked eyes even in the very low level of phosgene vapor. These results confirmed that the **DPA-CI** loaded test strip can be used for portable, visual, and reliable sensing of phosgene gas based on AIE processes.

3.5. The selectivity of the test strip for phosgene.

A good sensor should have excellent selectivity, to evaluate the selectivity of the **DPA-CI** loaded test strip for phosgene over several related gaseous contaminants, such as toluenesulfonyl chloride (TsCl), SO_2Cl_2 , SOCl_2 , POCl_3 , $\text{C}_2\text{Cl}_2\text{O}_2$, CH_3COCl , NH_3 , TEA, HCl, and diethyl chlorophosphate (DCP). The fluorescence spectra and the photos were collected. As shown in Fig. 6A and 6C, only in the presence of phosgene the test strips could induce significant fluorescence spectra and color change, while other related gaseous contaminants could not cause any obvious fluorescence spectra or color change compared to the control samples. Although some other acyl chlorides could couple with one $-\text{NH}$ group in **DPA-CI**, they cannot further combine with another amine group to form hexatomic cyclic urea. Thus, they cannot influence the fluorescence and absorption spectrum of **DPA-CI** due to the TICT behavior between 3-benzimidazole and the iminocoumarin unit cannot be inhibited and the conjugate system has not been prolonged. As a

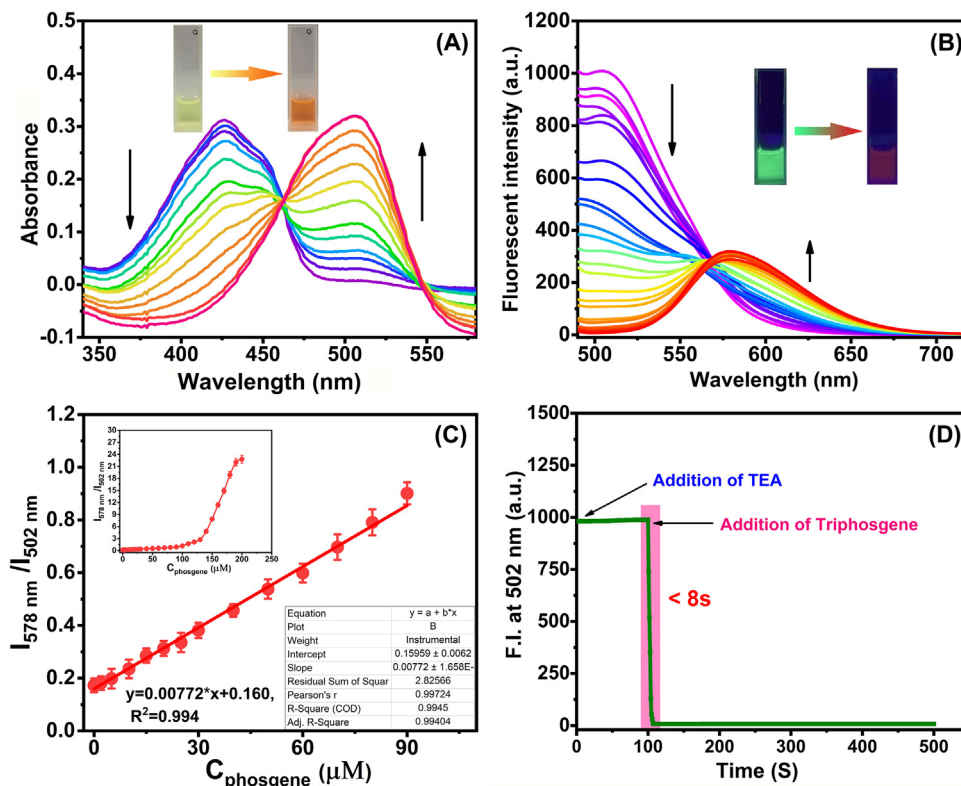


Fig. 4. (A) Absorption spectrum and (B) emission spectrum of **DPA-CI** (10 μM) in THF upon the addition of different amounts of phosgene (0–200 μM) for 1 min at 25 $^{\circ}\text{C}$. (C) The plot of the intensity ratio $I_{578\text{ nm}}/I_{502\text{ nm}}$ (inset) and linear relationships of **DPA-CI** (10 μM) vs different concentrations of phosgene in THF. (D) Time-dependent intensity response at 502 nm of **DPA-CI** (10 μM) with phosgene (200 μM) in THF. Excited at: 475 nm, slits: 10/10 nm.

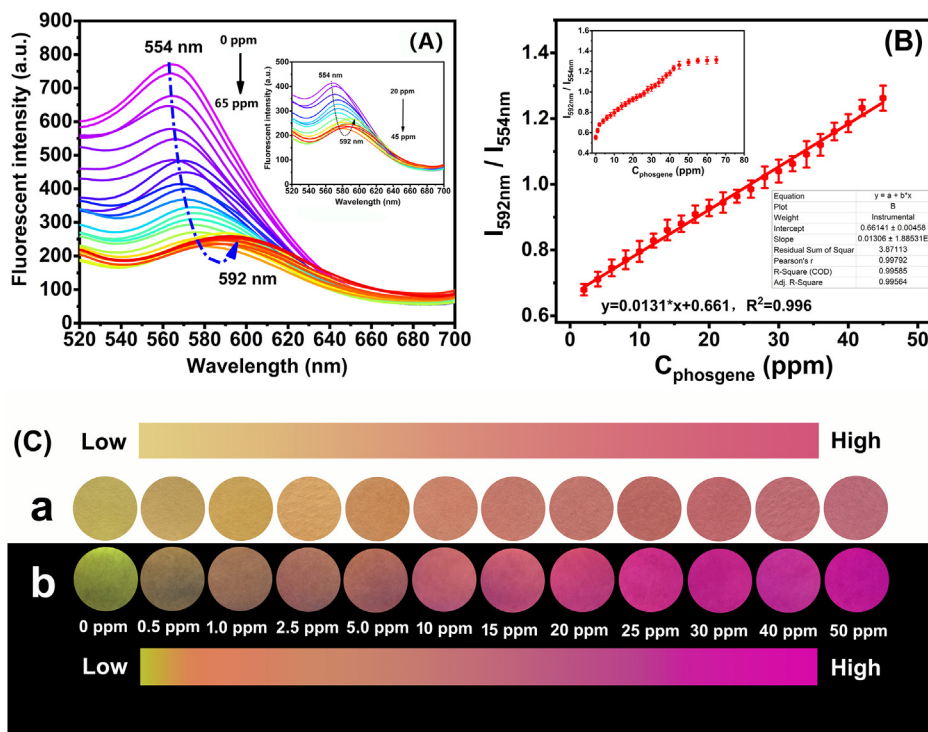


Fig. 5. (A) Fluorescent spectra of **DPA-CI** test strips in the presence of different amounts of gaseous phosgene for 2 min. Inset the fluorescence spectra from phosgene concentration 20 ppm to 45 ppm of **DPA-CI** (B) Linear correlation of the peak intensity ratio ($I_{592\text{ nm}}/I_{554\text{ nm}}$) of **DPA-CI** test strips vs the content of phosgene. Inset the peak intensity ratio of $I_{592\text{ nm}}/I_{554\text{ nm}}$ as a function of phosgene concentrations. Excited at: 365 nm. (C) Pictures of the color (a) and fluorescent color change (b) of **DPA-CI** test strips in the presence of increasing content of phosgene vapor for 2 min at 25 $^{\circ}\text{C}$. Under a 365 nm lamp.

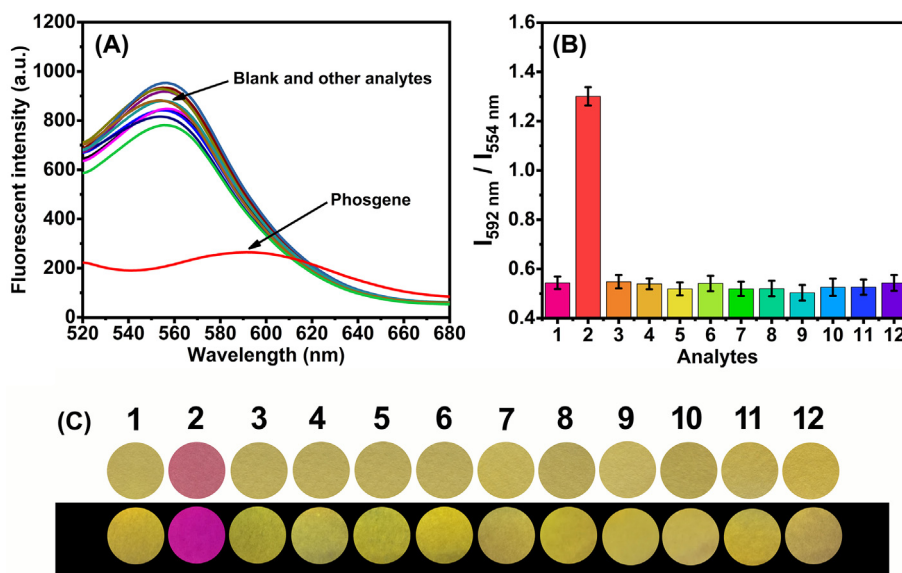


Fig. 6. (A) Fluorescent spectrum and (B) The peak intensity ratios ($I_{592\text{ nm}}/I_{554\text{ nm}}$) of **DPA-CI** test strips upon the addition of each analyte for 2 min. (1) air (blank), (2) phosgene, (3) toluenesulfonyl chloride (TsCl), (4) SO_2Cl_2 , (5) SOCl_2 , (6) POCl_3 , (7) $\text{C}_2\text{Cl}_2\text{O}_2$, (8) CH_3COCl , (9) NH_3 , (10) TEA, (11) HCl, (12) diethyl chlorophosphate (DCP). (C) The picture of the color (top) and fluorescent color change (bottom) of the test strips with the existence of different gaseous analytes.

result, the probe has better selectivity to phosgene molecule with two active reaction sites. In Fig. 6B, the intensity ratio ($I_{592\text{ nm}}/I_{554\text{ nm}}$) histogram further illustrates the excellent selectivity of the **DPA-CI** loaded test strip. These desirable results confirmed that the test strips made from **DPA-CI** can be a valuable portable sensor for a visual and sensitive monitor of phosgene gas.

3.6. Exploration of sensing mechanism

In the synthesis section, the reaction product (**DPA-CI-PS**) of **DPA-CI** with phosgene has been purified by column chromatography, and the molecular structure of **DPA-CI-PS** was fully characterized by ^1H NMR spectra and HR-MS. To further investigate the sensing mechanism, thin-layer chromatography (TLC) and ^1H NMR titration along with HR-MS titration of **TPE-CI** with phosgene in $\text{DMSO}-d_6$ were performed. As illustrated in Fig. 7A, the proton peak at 10.49, and 12.94 ppm were attached to the adjacent NH protons of Ha and Hb in the **DPA-CI** molecule, respectively. After phosgene bubbled into the **DPA-CI** solution, as seen in Fig. 7B, the proton peaks of Ha and Hb disappeared due to the two active -NH groups reacted with phosgene and generated hexatomic cyclic urea. Also, the generation of the product via the ^1H NMR titration was further confirmed by HR-MS (Figure S16), where two dominant peaks at m/z value of 455.1507 ($\text{M} + \text{H}^+$) and 477.1322 ($\text{M} + \text{Na}^+$), which confirmed the expected product m/z value at 454.1430 (calculated by ChemDraw software). Besides, the TLC analysis (Figure. S17) intuitively verified the product changes in the sensing process. Finally, combined with the previous DFT results for photophysical properties change, the possible sensing mechanism of the sensor **DPA-CI** for phosgene was followed proposed in Figure. S18.

4. Conclusion

In conclusion, we have successfully developed a diphenylamine-iminocoumarin-3-benzo[d]imidazole based fluorescent sensor **DPA-CI** for portable and visual recognition of highly toxic phosgene. The sensor undergoes TICT and AIE process transforms through twice carbamylation reactions with phosgene in solution or the solid-state test strips. More interestingly, the sensi-

tivity and rapid colorimetric and ratiometric fluorescence sensing process and be finished within 8 s in solution and 2 min in gaseous states, and the LOD can be calculated less than 0.11 ppm in gaseous condition and 0.27 μM in solution. Especially, the sensor **DPA-CI** loaded test strip features excellent selectivity for phosgene over other potential interferes. As compared with the other probes in Table S2, based on the unique advantage of the AIE characteristics and obvious dual-modes color change, our strategy would present some helpful insights into the manageable development of AIE based long-wavelength solid-state colorimetric and ratiometric fluorescent sensors for convenient and visual recognition of highly toxic gaseous pollutants.

CRedit authorship contribution statement

Qinghua Hu: Formal analysis, Funding acquisition, Writing - review & editing. **Tao Gong:** Investigation, Writing - original draft, Formal analysis. **Yu Mao:** Software. **Qiang Yin:** Software, Formal analysis. **Yuyuan Wang:** Resources. **Hongqing Wang:** Conceptualization, Methodology, Funding acquisition, Supervision, Validation, Writing - review & editing.

Declaration of Competing Interest

The authors declare that they have no known competing financial interests or personal relationships that could have appeared to influence the work reported in this paper.

Acknowledgements

Financial support from the National Natural Science Foundation of China (11804146, 11875161 and 51703075), and the Natural Science Foundation of Hunan Province (2020JJ5462), are gratefully acknowledged.

Appendix A. Supplementary data

Supplementary data to this article can be found online at <https://doi.org/10.1016/j.saa.2021.119589>.

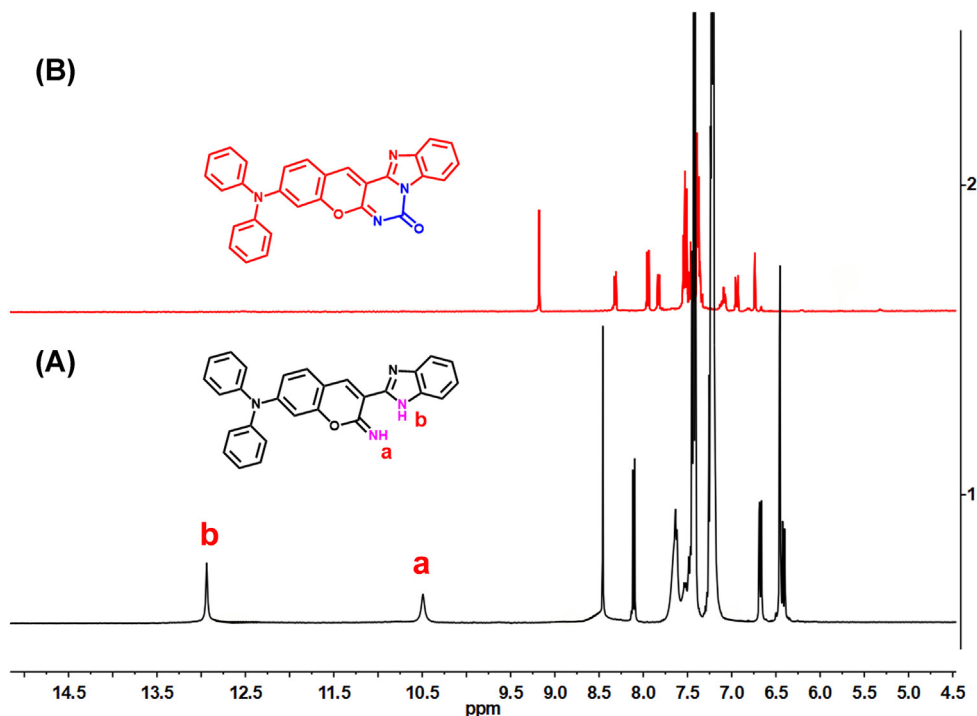


Fig. 7. ^1H NMR analysis of (A) DPA-CI in $\text{DMSO } d_6$ (B) DPA-CI after the addition of TEA and triphosgene in $\text{DMSO } d_6$.

References

- [1] M. Gutch, N. Jain, MohitMohan Singh, A. Agrawal, ArvindKumar Vaish, S. Consul, ShyamChand Chaudhary, Accidental phosgene gas exposure: A review with background study of 10 cases, *J Emerg Trauma Shock*. 6 (4) (2013) 271, <https://doi.org/10.4103/0974-2700.120372>.
- [2] S. Huang, B. Yan, S. Wang, X. Ma, Recent advances in dialkyl carbonates synthesis and applications, *Chem. Soc. Rev.* 44 (10) (2015) 3079–3116.
- [3] L. Chen, D.i. Wu, J. Yoon, Recent Advances in the Development of Chromophore-Based Chemosensors for Nerve Agents and Phosgene, *ACS Sens.* 3 (1) (2018) 27–43.
- [4] W.W. Holmes, B.M. Keyser, D.C. Paradiso, R. Ray, D.K. Andres, B.J. Benton, C.C. Rothwell, H.M. Hoard-Fruchey, J.F. Dillman, A.M. Sciuto, D.R. Anderson, Conceptual approaches for treatment of phosgene inhalation-induced lung injury, *Toxicol. Lett.* 244 (2016) 8–20.
- [5] L. Karalliedde, H. Wheeler, R. Maclehoose, V. Murray, Possible immediate and long-term health effects following exposure to chemical warfare agents, *Public Health* 114 (2000) 238–248.
- [6] L. Cotarca, T. Geller, J. Répási, Bis(trichloromethyl)carbonate (BTC, Triphosgene): A Safer Alternative to Phosgene?, *Org. Process Res. Dev.* 21 (9) (2017) 1439–1446.
- [7] S.L. Bartelt-Hunt, D.R.U. Knappe, M.A. Barlaz, A review of chemical warfare agent simulants for the study of environmental behavior, *Crit. Rev. Environ. Sci. Technol.* 38 (2) (2008) 112–136.
- [8] M. Davydova, M. Stuchlik, B. Rezek, K. Larsson, A. Kromka, Sensing of phosgene by a porous-like nanocrystalline diamond layer with buried metallic electrodes, *Sens. Actuator B-Chem.* 188 (2013) 675–680.
- [9] Y. Juillet, C. Dubois, F. Bintein, J. Dissard, A. Bossée, Development and validation of a sensitive thermal desorption–gas chromatography–mass spectrometry (TD-GC-MS) method for the determination of phosgene in air samples, *Anal. Bioanal. Chem.* 406 (21) (2014) 5137–5145.
- [10] G.H. Wei, H.X. Zhang, M. Zhao, H.B. Zhang, X. Yuan, Indirect Determination of Phosgene in Ambient Air by Reversed-Phase High Performance Liquid Chromatography, *Chemical Analysis and Meterage* 13 (2004) 23–25.
- [11] T. Wei, S. Lu, J. Sun, Z. Xu, X. Yang, F. Wang, Y. Ma, Y.S. Shi, X. Chen, Sanger's Reagent Sensitized Photocleavage of Amide Bond for Constructing Photocages and Regulation of Biological Functions, *J. Am. Chem. Soc.* 142 (8) (2020) 3806–3813.
- [12] S. Ghosh, J.R. Bhamore, N.I. Malek, Z.V.P. Murthy, S.K. Kailasa, Trypsin mediated one-pot reaction for the synthesis of red fluorescent gold nanoclusters: Sensing of multiple analytes (carbidopa, dopamine, Cu^{2+} , Co^{2+} and Hg^{2+} ions), *Spectrochim. Acta Pt. A-Molec. Biomolec. Spectr.* 215 (2019) 209–217.
- [13] Y. Yue, F. Huo, F. Cheng, X. Zhu, T. Mafireyi, R.M. Strongin, C. Yin, Functional synthetic probes for selective targeting and multi-analyte detection and imaging, *Chem. Soc. Rev.* 48 (15) (2019) 4155–4177.
- [14] Q. Hu, C. Yu, X. Xia, F. Zeng, S. Wu, A fluorescent probe for simultaneous discrimination of GSH and Cys/Hcy in human serum samples via distinctly-separated emissions with independent excitations, *Biosens. Bioelectron.* 81 (2016) 341–348.
- [15] S.P. Pandey, P.K. Singh, A polyelectrolyte based ratiometric optical sensor for Arginine and Lysine, *Sens. Actuator B-Chem.* 303 (2020) 127182.
- [16] A.M. Pettiwala, P.K. Singh, A molecular rotor based ratiometric sensor for basic amino acids, *Spectrochim. Acta Pt. A-Molec. Biomolec. Spectr.* 188 (2018) 120–126.
- [17] Y.u. Qi, Y. Huang, B. Li, F. Zeng, S. Wu, Real-time monitoring of endogenous cysteine levels in vivo by near-infrared turn-on fluorescent probe with large Stokes shift, *Anal. Chem.* 90 (1) (2018) 1014–1020.
- [18] Y. Zhou, S. Yang, J. Guo, H. Dong, K. Yin, W.T. Huang, R. Yang, In Vivo Imaging of Hypoxia Associated with Inflammatory Bowel Disease by a Cytoplasmic Protein-Powered Fluorescence Cascade Amplifier, *Anal. Chem.* 92 (8) (2020) 5787–5794.
- [19] Q. Fang, X.X. Yue, S.H. Han, B.H. Wang, X.Z. Song, A rapid and sensitive fluorescent probe for detecting hydrogen polysulfides in living cells and zebra fish, *Spectrochim. Acta Pt. A-Molec. Biomolec. Spectr.* 224 (2020) 117410.
- [20] H.B. Xiao, W. Zhang, P. Li, W. Zhang, X. Wang, B. Tang, Versatile Fluorescent Probes for Imaging the Superoxide Anion in Living Cells and In Vivo, *Angew. Chem. Int. Edit.* 59 (2020) 4216–4230.
- [21] D. Cheng, J. Peng, Y. Lv, D. Su, D. Liu, M. Chen, L. Yuan, X. Zhang, De novo design of chemical stability near-infrared molecular probes for high-fidelity hepatotoxicity evaluation in vivo, *J. Am. Chem. Soc.* 141 (15) (2019) 6352–6361.
- [22] X. Yue, J. Wang, J. Han, B. Wang, X. Song, A dual-ratiometric fluorescent probe for individual and continuous detection of H_2S and HClO in living cells, *Chem. Commun.* 56 (19) (2020) 2849–2852.
- [23] J.R. Bhamore, S. Jha, T.J. Park, S.K. Kailasa, Fluorescence sensing of Cu^{2+} ion and imaging of fungal cell by ultra-small fluorescent carbon dots derived from *Acacia concinna* seeds, *Sens. Actuator B-Chem* 277 (2018) 47–54.
- [24] X.B. Xu, W. Chen, M. Yang, X.J. Liu, F.L. Wang, R.Q. Yu, J.H. Jiang, Mitochondrial-targeted near-infrared fluorescence probe for selective detection of fluoride ions in living cells, *Talanta* 204 (2019) 655–662.
- [25] X. Wu, Q. Huang, Y.u. Mao, X. Wang, Y. Wang, Q. Hu, H. Wang, X. Wang, Sensors for determination of uranium: a review, *TrAC-Trend Anal. Chem.* 118 (2019) 89–111.
- [26] Y.H. Yan, X.Y. He, L. Su, J.Y. Miao, B.X. Zhao, A new FRET-based ratiometric fluorescence probe for hypochlorous acid and its imaging in living cells, *Talanta* 201 (2019) 330–334.
- [27] Y. Li, K.-N. Wang, L. He, L.-N. Ji, Z.-W. Mao, Synthesis, photophysical and anticancer properties of mitochondria-targeted phosphorescent cyclometalated iridium (III) N-heterocyclic carbene complexes, *J. Inorg. Biochem.* 205 (2020) 110976.
- [28] L. Wu, A.C. Sedgwick, X. Sun, S.D. Bull, X.-P. He, T.D. James, Reaction-Based Fluorescent Probes for the Detection and Imaging of Reactive Oxygen, Nitrogen, and Sulfur Species, *Acc. Chem. Res.* 52 (9) (2019) 2582–2597.
- [29] A.C. Sedgwick, J.T. Brewster, P. Harvey, A. Di, G.S. Iovan, X.-P. He, H. Tian, J.L. Sessler, T.D. James, Metal-based imaging agents: progress towards

- interrogating neurodegenerative disease, *Chem. Soc. Rev.* 49 (2020) 2886–2915.
- [30] L. Bai, W. Feng, G. Feng, An ultrasensitive fluorescent probe for phosgene detection in solution and in air, *Dyes Pigment.* 163 (2019) 483–488.
- [31] Y. Hu, X. Zhou, H. Jung, S.-J. Nam, M.H. Kim, J. Yoon, Colorimetric and fluorescent detecting phosgene by a second-generation chemosensor, *Anal. Chem.* 90 (5) (2018) 3382–3386.
- [32] H. Xie, Y. Wu, F. Zeng, J. Chen, S. Wu, An AIE-based fluorescent test strip for the portable detection of gaseous phosgene, *Chem. Commun.* 53 (70) (2017) 9813–9816.
- [33] K. Maiti, D. Ghosh, R. Maiti, V. Vyas, P. Datta, D. Mandal, D.K. Maiti, Ratiometric chemodosimeter: an organic-nanofiber platform for sensing lethal phosgene gas, *J. Mater. Chem. A* 7 (2019) 1756–1767.
- [34] Q. Hu, C. Duan, J. Wu, D. Su, L. Zeng, R. Sheng, Colorimetric and ratiometric chemosensor for visual detection of gaseous phosgene based on anthracene carboxyimide membrane, *Anal. Chem.* 90 (14) (2018) 8686–8691.
- [35] Y. Hu, L. Chen, H. Jung, Y. Zeng, S. Lee, K.M.K. Swamy, X. Zhou, M.H. Kim, J. Yoon, Effective strategy for colorimetric and fluorescence sensing of phosgene based on small organic dyes and nanofiber platforms, *ACS Appl. Mater. Interfaces* 8 (34) (2016) 22246–22252.
- [36] S.-L. Wang, C. Li, Q.-H. Song, Fluorescent chemosensor for dual-channel discrimination between phosgene and triphosgene, *Anal. Chem.* 91 (9) (2019) 5690–5697.
- [37] H.-C. Xia, X.-H. Xu, Q.-H. Song, Fluorescent chemosensor for selective detection of phosgene in solutions and in gas phase, *ACS Sens.* 2 (1) (2017) 178–182.
- [38] Y. Zhang, A. Peng, X. Jie, Y. Lv, X. Wang, Z. Tian, A BODIPY-based fluorescent probe for detection of subnanomolar phosgene with rapid response and high selectivity, *ACS Appl. Mater. Interfaces* 9 (16) (2017) 13920–13927.
- [39] W. Feng, S. Gong, E. Zhou, X. Yin, G. Feng, Readily prepared iminocoumarin for rapid, colorimetric and ratiometric fluorescent detection of phosgene, *Anal. Chim. Acta* 1029 (2018) 97–103.
- [40] Y.L. Huang, W. Ye, Y.T. Su, Z.Y. Wu, H. Zheng, A naphthalimide-based probe for phosgene sensing based on the phosgene-induced beckmann rearrangement, *Dyes Pigment.* 173 (2019) 107854.
- [41] C. Wu, H. Xu, Y. Li, R. Xie, P. Li, X. Pang, Z. Zhou, B. Gu, H. Li, Y. Zhang, An ES IPT-based fluorescent probe for the detection of phosgene in the solution and gas phases, *Talanta* 200 (2019) 78–83.
- [42] M. Sayar, E. Karakaş, T. Güner, B. Yildiz, U.H. Yildiz, M. Emrullahoğlu, A BODIPY-Based Fluorescent Probe to Visually Detect Phosgene: Toward the Development of a Handheld Phosgene Detector, *Chem.-Eur. J.* 24 (2018) 3136–3140.
- [43] X. Zhou, Y. Zeng, C. Liyan, X. Wu, J. Yoon, A Fluorescent Sensor for Dual-Channel Discrimination between Phosgene and a Nerve-Gas Mimic, *Angew. Chem. Int. Edit.* 55 (15) (2016) 4729–4733.
- [44] L. Chen, D.i. Wu, J.-M. Kim, J. Yoon, An ES IPT-based fluorescence probe for colorimetric, ratiometric, and selective detection of phosgene in solutions and the gas phase, *Anal. Chem.* 89 (22) (2017) 12596–12601.
- [45] S.-L. Wang, C.-L. Zhang, Q.-H. Song, Selectively instant-response nanofibers with a fluorescent chemosensor toward phosgene in gas phase, *J. Mater. Chem. C* 7 (6) (2019) 1510–1517.
- [46] P. Liu, N.a. Liu, C. Liu, Y. Jia, L. Huang, G. Zhou, C. Li, S. Wang, A colorimetric and ratiometric fluorescent probe with ultralow detection limit and high selectivity for phosgene sensing, *Dyes Pigment.* 163 (2019) 489–495.
- [47] T.-I. Kim, B. Hwang, J. Bouffard, Y. Kim, Instantaneous colorimetric and fluorogenic detection of phosgene with a meso-oxime-BODIPY, *Anal. Chem.* 89 (23) (2017) 12837–12842.
- [48] S.-L. Wang, L. Zhong, Q.-H. Song, Sensitive and Selective Detection of Phosgene, Diphosgene, and Triphosgene by a 3, 4-Diaminonaphthalimide in Solutions and the Gas Phase, *Chem.-Eur. J.* 24 (21) (2018) 5652–5658.
- [49] M. Du, B. Huo, J. Liu, M. Li, A.o. Shen, X. Bai, Y. Lai, L. Fang, Y. Yang, A turn-on fluorescent probe based on Si-rhodamine for sensitive and selective detection of phosgene in solution and in the gas phase, *J. Mater. Chem. C* 6 (39) (2018) 10472–10479.
- [50] T.-I. Kim, D. Kim, J. Bouffard, Y. Kim, Rapid, specific, and ultrasensitive fluorogenic sensing of phosgene through an enhanced PeT mechanism, *Sens. Actuator B-Chem.* 283 (2019) 458–462.
- [51] S. Wang, B.T. Zhu, B.Y. Wang, P.W. Fan, Y.X. Jiu, M. Zhang, L.R. Jiang, J.-T. Hou, A highly selective phenothiazine-based fluorescent chemosensor for phosgene, *Dyes Pigment.* 173 (2020) 107933.
- [52] Q.H. Hu, Q.X. Huang, K.X. Liang, Y.Y. Wang, Y. Mao, Q. Yin, H.Q. Wang, An AIE +TICT activated colorimetric and ratiometric fluorescent sensor for portable, rapid, and selective detection of phosgene, *Dyes Pigment.* 176 (2020) 108229.
- [53] X.-Z. Wei, Y.-L. Fu, M.-J. Xue, Q.-H. Song, Synthesis of Oxadiazolones with Hydrazides: The Mechanism and the Sensing Application as Sensitive, Rapid, and Visual Fluorescent Sensors for Phosgene, *Org. Lett.* 21 (2019) 9497–9501.
- [54] H.-C. Xia, X.-H. Xu, Q.-H. Song, BODIPY-based fluorescent sensor for the recognition of phosgene in solutions and in gas phase, *Anal. Chem.* 89 (7) (2017) 4192–4197.
- [55] S.-L. Wang, L. Zhong, Q.-H. Song, A ratiometric fluorescent chemosensor for selective and visual detection of phosgene in solutions and in the gas phase, *Chem. Commun.* 53 (9) (2017) 1530–1533.
- [56] J. Luo, Z. Xie, J.W.Y. Lam, L. Cheng, B.Z. Tang, H. Chen, C. Qiu, H.S. Kwok, X. Zhan, Y. Liu, D. Zhu, Aggregation-induced emission of 1-methyl-1, 2, 3, 4, 5-pentaphenylsilole, *Chem. Commun.* (18) (2001) 1740–1741, <https://doi.org/10.1039/b105159h>.
- [57] J. Wang, C. Li, Q. Chen, H. Li, L. Zhou, X. Jiang, M. Shi, P. Zhang, G. Jiang, B.Z. Tang, An Easily Available Ratiometric Reaction-Based AIE Probe for Carbon Monoxide Light-up Imaging, *Anal. Chem.* 91 (15) (2019) 9388–9392.
- [58] J. Li, J.X. Wang, H.X. Li, N. Song, D. Wang, B.Z. Tang, Supramolecular materials based on AIE luminogens (AIEgens): construction and applications, *Chem. Soc. Rev.* 49 (2020) 1144–1172.
- [59] Y.Y. Li, Z.C. Cai, S.J. Liu, H. Zhang, S.T.H. Wong, J.W.Y. Lam, R.T.K. Kwok, J. Qian, B.Z. Tang, Design of AIEgens for near-infrared IIb imaging through structural modulation at molecular and morphological levels, *Nat. Commun.* 11 (2020) 1–10.
- [60] Y. Liu, J. Nie, J. Niu, W. Wang, W. Lin, An AIE+ESIPT ratiometric fluorescent probe for monitoring sulfur dioxide with distinct ratiometric fluorescence signals in mammalian cells, mouse embryonic fibroblast and zebrafish, *J. Mater. Chem. B* 6 (13) (2018) 1973–1983.
- [61] Z. Guo, C. Yan, W.-H. Zhu, High-Performance Quinoline-Malononitrile Core as a Building Block for the Diversity-Oriented Synthesis of AIEgens, *Angew. Chem. Int. Ed.* 59 (25) (2020) 9812–9825.
- [62] T. Yang, Y. Zuo, Y.u. Zhang, Z. Gou, X. Wang, W. Lin, AIE-active polysiloxane-based fluorescent probe for identifying cancer cells by locating lipid drops, *Anal. Chim. Acta* 1091 (2019) 88–94.
- [63] W. Fu, C.X. Yan, Z.Q. Guo, J.J. Zhang, H.Y. Zhang, H. Tian, W.H. Zhu, Rational Design of Near-Infrared Aggregation-Induced-Emission-Active Probes. In Situ Mapping of Amyloid- β Plaques with Ultrasensitivity and High-Fidelity, *J. Am. Chem. Soc.* 141 (2019) 3171–3177.
- [64] R. Zhang, Y. Duan, B. Liu, Recent advances of AIE dots in NIR imaging and phototherapy, *Nanoscale* 11 (41) (2019) 19241–19250.
- [65] J.Y. Gong, J.L. Han, Q. Liu, X.J. Ren, P.F. Wei, L. Yang, Y. Zhang, J. Liu, Y.Q. Dong, Y. G. Wang, X.Z. Song, B.Z. Tang, An ideal platform of light-emitting materials from phenothiazine: facile preparation, tunable red/NIR fluorescence, bent geometry-promoted AIE behaviour and selective lipid-droplet (LD) tracking ability, *J. Mater. Chem. C* 7 (2019) 4185–4190.
- [66] S.J. Liu, X. Zhou, H.K. Zhang, H.L. Ou, J.W.Y. Lam, Y. Liu, L.Q. Shi, D. Ding, B.Z. Tang, Molecular Motion in Aggregates: Manipulating TICT for Boosting Photothermal Theranostics, *J. Am. Chem. Soc.* 141 (2019) 5359–5368.
- [67] M. Jiang, X. Gu, J.W.Y. Lam, Y. Zhang, R.T.K. Kwok, K.S. Wong, B.Z. Tang, Two-photon AIE bio-probe with large Stokes shift for specific imaging of lipid droplets, *Chem. Sci.* 8 (8) (2017) 5440–5446.
- [68] X.L. Cai, B. Liu, Aggregation-Induced Emission: Recent Advances in Materials and Biomedical Applications, *Angew. Chem. Int. Ed.* 59 (2020) 9868–9886.
- [69] N.H. Mudliar, P.M. Dongre, P.K. Singh, A molecular rotor based dual ratiometric sensor for heparinase, *Dyes Pigment.* 182 (2020) 108528.
- [70] S.P. Pandey, P.K. Singh, A ratiometric scheme for the fluorescent detection of protamine, a heparin antidote, *J. Mol. Liq.* 303 (2020) 112589.
- [71] V.R. Singh, P.K. Singh, A supramolecule based fluorescence turn-on and ratiometric sensor for ATP in aqueous solution, *J. Mat. Chem. B* 8 (2020) 1182–1190.
- [72] N.H. Mudliar, P.M. Dongre, P.K. Singh, An efficient J-aggregate based fluorescence turn-on and ratiometric sensor for heparin, *Sens. Actuator B-Chem.* 301 (2019) 127089.
- [73] A.M. Desai, P.K. Singh, Ratiometric fluorescence turn-on sensing of perchlorate anion, a non-radioactive surrogate of hazardous perchlorate, in aqueous solution, *Sens. Actuator B-Chem.* 277 (2018) 205–209.
- [74] M.K. Leung, C.C. Chang, M.H. Wu, K.H. Chuang, J.H. Lee, S.J. Shieh, S.C. Lin, C.F. Chiu, 6-N, N-Diphenylaminobenzofuran-Derived Pyran Containing Fluorescent Dyes: A New Class of High-Brightness Red-Light-Emitting Dopants for OLED, *Org. Lett.* 8 (2006) 2623–2626.